Geophysical Research Letters

RESEARCH LETTER
10.1029/2018GL078340

Key Points:
- A remote sensing technique is proposed to estimate the reconnection electric field using in situ multipoint observations at the separatrix
- The proposed technique is successfully applied to virtual observations in a 2-D fully kinetic particle-in-cell simulation
- The technique is also applied to a magnetotail MMS event during an intense substorm, and the result shows a large reconnection electric field

Supporting Information:
- Supporting Information S1

Correspondence to:
T. K. M. Nakamura,
takuma.tkm.nakamura@gmail.com

Citation:
Nakamura, T. K. M., Nakamura, R., Varsani, A., Genestreti, K. J., Baumjohann, W., & Liu, Y.-H. (2018). Remote sensing of the reconnection electric field from in situ multipoint observations of the separatrix boundary. *Geophysical Research Letters*, *45*, 3829–3837. https://doi.org/10.1029/2018GL078340

Received 12 APR 2018
Accepted 18 APR 2018
Accepted article online 30 APR 2018
Published online 9 MAY 2018

Remote Sensing of the Reconnection Electric Field From In Situ Multipoint Observations of the Separatrix Boundary

T. K. M. Nakamura[1], R. Nakamura[1], A. Varsani[1,2], K. J. Genestreti[1], W. Baumjohann[1], and Y.-H. Liu[3]

[1]Space Research Institute, Austrian Academy of Sciences, Graz, Austria, [2]Mullard Space Science Laboratory, UCL, Dorking, UK, [3]Department of Physics and Astronomy, Dartmouth College, Hanover, NH, USA

Abstract A remote sensing technique to infer the local reconnection electric field based on in situ multipoint spacecraft observation at the reconnection separatrix is proposed. In this technique, the increment of the reconnected magnetic flux is estimated by integrating the in-plane magnetic field during the sequential observation of the separatrix boundary by multipoint measurements. We tested this technique by applying it to virtual observations in a two-dimensional fully kinetic particle-in-cell simulation of magnetic reconnection without a guide field and confirmed that the estimated reconnection electric field indeed agrees well with the exact value computed at the X-line. We then applied this technique to an event observed by the Magnetospheric Multiscale mission when crossing an energetic plasma sheet boundary layer during an intense substorm. The estimated reconnection electric field for this event is nearly 1 order of magnitude higher than a typical value of magnetotail reconnection.

Plain Language Summary Magnetic reconnection is an important phenomenon in space plasmas that explosively releases the accumulated magnetic energy. In the Earth's magnetotail, it is known that the released energy by this process leads to aurora substorms. The rate of reconnection, which defines how efficiently the magnetic flux is transferred at the central reconnection region called the diffusion region, is a key parameter to explore such reconnection physics. However, it is very challenging to directly measure this parameter by observing the small-scale diffusion region in situ. Thus, in this paper, we propose a new remote sensing technique that infers the reconnection rate along the boundary of the whole reconnection region called the separatrix from in situ measurements. In this technique, by observing how rapidly the magnetic flux passes through the separatrix, the rate can be remotely inferred even outside the diffusion region. We confirmed the adequacy of this technique by testing it in a kinetic simulation, and then applied it to a latest observation event by the MMS spacecraft during an intense substorm. The result shows a remarkably high rate. This indicates the positive correlation between the reconnection rate and the substorm strength and strongly motivates future survey using the technique proposed in this paper.

1. Introduction

Magnetic reconnection is a key explosive phenomenon in collisionless plasmas that converts magnetic energy to plasma kinetic energies through a change in the magnetic field topology. The topological change occurs in a small-scale region surrounding the reconnection X-line called the diffusion region where plasmas are decoupled from the magnetic field. The ratio between the inflowing and outflowing plasma speeds $R = V_{in}/V_{out}$ is a key parameter that defines how efficiently the topology change occurs. Considering the Faraday's law and the pressure balance between the inflow and outflow regions, this so-called dimensionless or normalized reconnection rate essentially corresponds to the out-of-plane component of the normalized electric field near the diffusion region $R \sim cE_y/(V_A B_0)$ where B_0 is the amplitude of the reconnecting field and V_A is the Alfvén speed. This E_y component, which is commonly referred to as the reconnection electric field E_r or the unnormalized reconnection rate, is also a key parameter to evaluate how rapidly the magnetic flux is transferred from the inflow to outflow regions. The main focus of this paper is to estimate the E_r value from in situ multipoint spacecraft observations.

Fast reconnection with a large normalized reconnection rate of the order 0.1 is required to explain global energy release during various explosive phenomena such as solar flares and geomagnetic substorms

(Cassak et al., 2017). Past theoretical models in the magnetohydrodynamic (MHD) regime, such as the Sweet-Parker model (Parker, 1957; Sweet, 1958) and the Petschek model (Petschek, 1964), suggested that the reconnection rate is controlled by the Lundquist number $S = LV_A/\eta$. Here L is the scale length of the diffusion region and η is the resistivity. Although a fast rate can be accomplished only by a limited Lundquist number in these theoretical models, past numerical studies comparing various simulation models from MHD to fully kinetic models suggested that the decoupling of ion and electron dynamics (i.e., the Hall effect) in collisionless plasmas commonly facilitates the fast reconnection and makes the normalized rate of order 0.1 (e.g., Birn et al., 2001; Shay et al., 2001). Some recent numerical studies also demonstrated a similar fast rate even in regimes where the Hall effect is negligible (Liu et al., 2014, and references therein), while some other studies demonstrated extremely larger (>0.1) rates from combinations with an interchange instability (Birn et al., 2015) and the Kelvin-Helmholtz instability (Nakamura, Eriksson, et al., 2017). More recently, Liu et al. (2017) showed that the value of fast rate could be explained by the constraint imposed at the inflow and outflow regions. In their theory, the fast rate of order 0.1 appears over a wide range of the exhaust opening angle.

Considering flux conservation, the flux flowing into the diffusion region balances the flux out of the diffusion region, which gives the reconnection electric field as $E_r \sim RV_AB_0/c \sim V_{in}B_{in}/c \sim V_{out}B_{out}/c$. From this relation, assuming $B_{in} \sim B_0$ and $V_{out} \sim V_A$, the normalized reconnection rate can be estimated as $R \sim V_{in}/V_A \sim B_{out}/B_0$. By directly measuring V_{in} and B_{out} at the Earth's magnetopause using the Cluster spacecraft, the normalized rate R was roughly estimated to be of an order 0.1 (e.g., Fuselier et al., 2010; Phan et al., 2001; Vaivads et al., 2004).

Near the center of the diffusion region, the reconnection electric field E_r is sustained by the nonideal electric field $E_y' = E_y + (\mathbf{V}_e \times \mathbf{B})_y$ (e.g., Hesse & Winske, 1998; Nakamura et al., 2016). The region near the center of the diffusion region with a finite E_y' is called the electron diffusion region (EDR). Recent high-resolution in situ observations by the Magnetospheric Multiscale (MMS) spacecraft (Burch, Moore, et al., 2016) successfully detected the EDR in some crossing events of the Earth's magnetopause (e.g., Burch, Torbert, et al., 2016; Genestreti et al., 2018) and found in such an EDR event that E_r near the EDR normalized by the upstream V_AB_0 was also of an order 0.1 (Chen et al., 2017).

Although these local observations estimated the reconnection electric field E_r and the corresponding normalized reconnection rate R around the diffusion region at the Earth's magnetopause, it is challenging to encounter the small-scale diffusion region and measure the rates therein. As we will show in the next section (section 2.1), we propose a new estimation technique that infers the local E_r using in situ multipoint measurement at the reconnection separatrix boundary. Since the cross section of the separatrix boundary is much larger than that of the diffusion region, it is expected for the separatrix to be crossed and observed by in situ measurements much more frequently. We confirmed the adequacy of this technique by applying it to a 2-D fully kinetic simulation of reconnection (section 3.2). We then tried to apply it to an MMS observation event on 10 August 2016 of the thin plasma sheet boundary layer (PSBL) in the magnetotail which was first reported by Nakamura, Nagai, et al. (2017), Nakamura et al. (2018) (section 4.2).

2. Methods

2.1. Remote Sensing Technique to Measure the Reconnection Electric Field

Considering a situation in which reconnection develops in the x-z plane and assuming that the three dimensionality is negligible, E_y at the X-line, which corresponds to the reconnection electric field E_r, can be described as

$$E_r \sim E_{y,x-\mathrm{line}} \sim -\frac{\partial A_{y,x-\mathrm{line}}}{\partial t}, \tag{1}$$

where $A_{y,x\text{-line}}$ is the y component of the vector potential at the X-line. Defining the separatrix as the boundary between the reconnected and unreconnected field lines, the potential is constant along the separatrix (Vasyliunas, 1975). Thus, the reconnection electric field can be remotely estimated even at the reconnection separatrix boundary by measuring the amount of the magnetic flux that crosses the boundary during a given time as

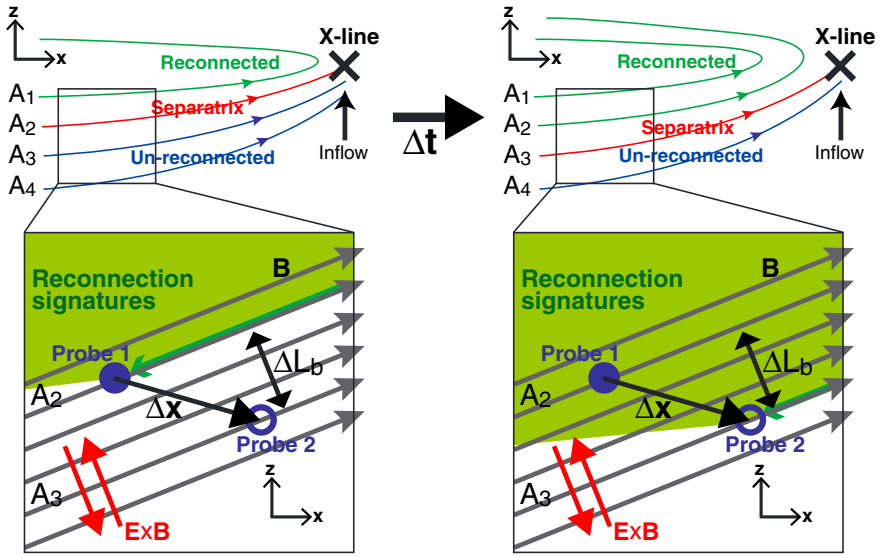

Figure 1. Schematic for evolution of steady 2-D reconnection in the *x-z* plane, in which the vector potential at the X-line and the separatrix evolves from A_2 to A_3 during Δt. When two probes with a small separation exist just outside this separatrix boundary, these probes are expected to sequentially observe a signature of the boundary as the boundary evolves during reconnection.

$$E_r \sim -\frac{\partial A_{y,x-\mathrm{line}}}{\partial t} \sim -\frac{\partial A_{y,\mathrm{separatrix}}}{\partial t}, \tag{2}$$

where $A_{y,\mathrm{separatrix}}$ is the y component of the vector potential along the separatrix.

Figure 1 is a schematic illustrating the evolution of 2-D reconnection in the *x-z* plane, in which $A_{y,\mathrm{separatrix}}$ ($=A_{y,x\text{-line}}$) evolves from A_2 to A_3 during Δt. By assuming the constant reconnection rate during Δt, the peak E_r can be estimated as $E_r \sim -(A_3 - A_2)/\Delta t$. We consider a situation in which two probes are separated by $\Delta \mathbf{x} = \mathbf{x}_2\text{-}\mathbf{x}_1 = (\Delta x, \Delta z)$, located on the magnetic field lines A_2 and A_3, and sequentially cross the reconnection boundary during Δt. In this situation, by assuming (i) the constant and uniform electric and magnetic field between the two probes and (ii) no convection of the field lines relative to the probes, the reconnected flux during Δt can be computed as $\Delta A_y = (A_3\text{-}A_2) = |\boldsymbol{B}|_{xz}\Delta L_b = (\Delta \boldsymbol{x} \times \boldsymbol{B})_{\boldsymbol{y}}$. Thus, after taking into account the potential convection of field lines at the $\mathbf{E} \times \mathbf{B}$ drift velocity $\boldsymbol{V}_c = (\boldsymbol{E} \times \boldsymbol{B})/B^2$, the reconnection electric field can be remotely estimated at the separatrix boundary as

$$E_r \sim -\frac{(\Delta \boldsymbol{X} \times \boldsymbol{B})_{\boldsymbol{y}}}{\Delta t} \sim [-(\boldsymbol{V}_{\mathrm{tim}} - \boldsymbol{V}_c) \times \boldsymbol{B}]_y \sim -B_x \frac{\Delta z}{\Delta t} + B_z \frac{\Delta x}{\Delta t} + B_x \left(\frac{\boldsymbol{E} \times \boldsymbol{B}}{B^2}\right)_z - B_z \left(\frac{\boldsymbol{E} \times \boldsymbol{B}}{B^2}\right)_x. \tag{3}$$

Here $\Delta \mathbf{X} = \Delta \boldsymbol{x} - \frac{\boldsymbol{E} \times \boldsymbol{B}}{B^2} \Delta t$ is the relative separation in the comoving frame of field lines. $\mathbf{V}_{\mathrm{tim}} = \Delta \mathbf{x}/dt$ is the timing velocity. Using this formalism, we can remotely estimate the reconnection electric field E_r from the difference between $\mathbf{V}_{\mathrm{tim}}$ and $\mathbf{V}_c$ at the reconnection boundary. We assume that the time delay by which the reconnection signatures propagate from the X-line to the observation point is negligible and that the propagation speed parallel to the boundary is much faster than the boundary motion perpendicular to the boundary ($V_{p\parallel} \gg |\boldsymbol{V}_{\mathrm{tim}} - \boldsymbol{V}_c|_{\perp}$). In other words, the boundary of the region filled with the reconnection signatures is assumed to be identical to the separatrix boundary and move only in the perpendicular direction.

It should be noted that similar methods to infer E_r from ground-based observations have been proposed (e.g., Vasyliunas, 1984; de la Beaujardière et al., 1991) and applied to various magnetotail reconnection events (e.g., Blanchard et al., 1997, Hubert et al., 2006; Freeman et al., 2007), in which the velocity of separatrix motion (corresponding to $\mathbf{V}_{\mathrm{tim}}$ in equation (3)) is calculated by tracing the location of the open/closed field line boundary in the ionosphere. While these ground-based observations reasonably resolved the global flux transfer rate of 1–10 min, the technique proposed in this paper can resolve the local rate, which cannot be resolved by ground-based observations.

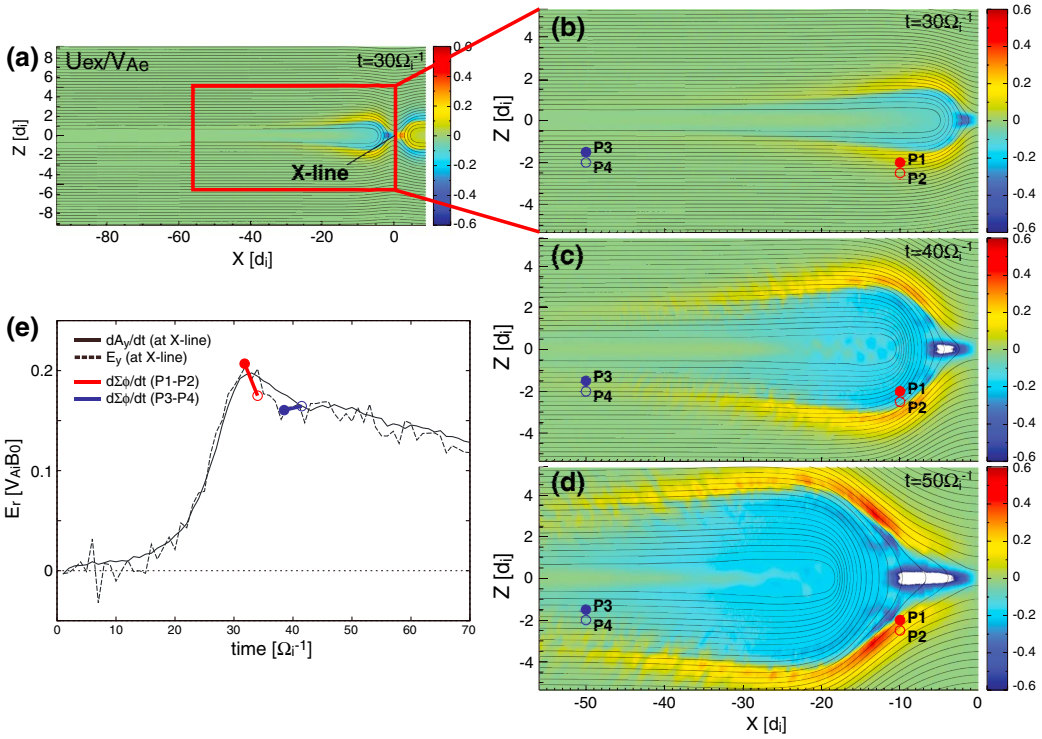

Figure 2. (a) U_{ex} contour in the *x*-*z* plane at $t = 30\Omega_i^{-1}$. (b–d) Time evolution of zoomed-in views of U_{ex} contours from $t = 30$ to $50\Omega_i^{-1}$. The color range of Figures 2b–2d is fixed as $[-0.6V_{Ae}, 0.6V_{Ae}]$ to visualize the small amplitude of U_{ex} variations. The red and blue circles indicate locations of the virtual probes P1–P4 for virtual observations shown in Figure 3. (e) Time evolution of the reconnection electric field E_r measured at the X-line by the time deviation of A_y (solid) and E_y (dashed). The red and blue bars show the reconnection rates remotely estimated by the pairs of virtual observation probes P1-P2 and P3-P4, respectively.

2.2. Simulation Setup

To apply the proposed remote sensing technique to numerical simulations of magnetic reconnection, we employ the fully kinetic explicit particle-in-cell (PIC) code EM3D (cf., Hoshino, 1987; Nakamura et al., 2016). The simulation performed in this paper is 2–1/2 dimensional in the *x*-*z* plane. The initial parameters are basically the same as the ones employed in the Geospace Environmental Modeling (GEM) magnetic reconnection challenge (Birn et al., 2001; Pritchett, 2001) but for a much larger system size. The initial magnetic field and the corresponding number density profiles are set up as $B_x(z) = B_{x0}\tanh(z/L_0)$ (Harris sheet) and $n_i(z) = n_e(z) = n_0\mathrm{sech}^2(z/L_0) + n_b$, where L_0 is the half-thickness of the initial current sheet and n_0 and n_b are the Harris and background density components, respectively. L_0 is set to be $0.75d_i$, where $d_i = c/\omega_{pi}$ is the ion inertial length based on n_0. n_b is set to be $0.2n_0$. The ratio between the electron plasma frequency and the gyrofrequency is set to be $\omega_{pe}/\Omega_e = 2.0$. The ion-to-electron temperature ratio is set to be $T_i/T_e = 5$. The ion-to-electron mass ratio is $m_i/m_e = 25$. The system size based on d_i is set to be $(L_x, L_z) = (224d_i, 51.2d_i)$, which minimize the effects from the simulation boundaries during the simulation times shown in this paper. The boundary conditions are periodic along the *x* direction, with conducting walls along the *z* direction. A Gaussian-type initial magnetic field perturbation is added at the center of the simulation domain according to $\delta\mathbf{B} = z \times \nabla\Phi$, where $\Phi = -0.1B_{x0}\exp[-(x/5D_0)^2]\exp[-(z/D_0)^2]$ to ensure that reconnection starts and evolves from only a single X-line at $x = 0$.

3. Results

3.1. Overview of the Simulation Results

Figures 2a–2d show the time evolution of the *x* component of the electron bulk flow velocity. The electron outflow jet (see deepest blue-colored region around $z \sim 0$ in Figures 2b–2d) evolves and expands in the *x* direction, as has been shown in past fully kinetic simulations with sufficiently large system sizes (e.g., Karimabadi et al., 2007; Shay et al., 2007). In addition to the electron outflow jet, the boundaries of the

reconnection region also expand in both the x and z directions. These boundaries feature electrons streaming away from the X-line along the separatrix (see deeper blue-colored regions near the separatrix in Figures 2b–2d) and return flows (see yellow-to-red colored regions locating just outside the blue colored regions), which produce the Hall B_y enhancements along the separatrix.

Figure 2e shows the reconnection electric field E_r measured at the X-line by $\partial A_y/\partial t$ (solid) and E_y (dashed), respectively. E_r reaches the maximum value ~$0.2V_{Ai}B_0$ at $t \sim 30\Omega_i^{-1}$ and remains larger than $0.1V_{Ai}B_0$ after the saturation, as seen in past kinetic simulations with large system sizes (e.g., Daughton et al., 2006). The blue and red bars in Figure 2e are the values remotely estimated from the virtual observation probes P1–P4 marked in Figures 2b–2d, as we will show in the next section.

3.2. Remote Sensing of the Reconnection Electric Field

To apply the remote sensing technique to the simulation, we performed virtual observations in the simulation, in which two pairs of virtual observation probes are put at two different distances from the X-line ($x = -10d_i$ for the P1–P2 pair and $x = -50d_i$ for the P3–P4 pair) as marked in Figures 2b–2d, both of which locate outside the diffusion region (see Figure S1). The two probes for both P1-P2 and P3-P4 pairs are separated by $0.5d_i = (2.5d_e)$ in the z direction. The P1-P2 pair first enters the Hall current system from the lobe region due to the expansion of the boundary mainly toward the $-z$ direction, and then exits the system due to the evolution of the reconnection layer in both the $-x$ and $-z$ direction. The P3-P4 pair enters the reconnection region when the parallel electron beam reaches the probe locations, which is the first contact of the reconnection signature from the X-line.

Figures 3a–3f show the virtual observation results for the P1-P2 pair. The P1 probe, which is closer to the neutral point than P2, first observes the inflowing low-energy ($<0.1m_ec^2$) electrons, which create the positive U_{ex} peak at $t \sim 31.5\Omega_i^{-1}$ (see Figures 3b and 3f). P1 then observes the outflowing higher energy electrons and the corresponding negative U_{ex} (see Figures 3a and 3f). These electron flows carry currents and provide the B_y enhancement as seen in Figure 3e, which are the typical signatures of the Hall current system (e.g., Nagai et al., 2003). The P2 probe observes similar signatures $\Delta t = 1.5\Omega_i^{-1}$ later than P1 (see the duration between two vertical lines in Figures 3a–3f, which show the observation times of $B_y = 0.1B_0$ for P1 and P2). Substituting this Δt, the separation Δz, and the observed convection velocity (cyan lines in Figure 3f) into equation (3), the reconnection electric field E_r is estimated as shown in red marks in Figure 2e. Note that the times of the two marks correspond to the times of the two vertical lines shown in Figures 3a–3f. The filled circle is the estimated E_r using the values observed at the time of the $B_y = 0.1B_0$ crossing for P1, while the open circle is for P2. Since equation (3) assumes the constant field during the observation interval, the difference of the two circles corresponds to the error of the estimation.

Figures 3g–3l show the virtual observation results for the P3-P4 pair. The P3 probe, which is closer to the neutral point than P4, first observes the high energy ($>0.1m_ec^2$) parallel electron beam flowing away from the X-line (Figure 3g). After the first contact of the highest energy electrons, the lower energy electrons are sequentially observed and form the energy dispersion (see the time after the first vertical line in Figure 3g). This dispersion is caused mainly by the time-of-flight effect in which slower electrons reach the probe later than the faster electrons when these electrons are coming from a close location near the X-line along the same field line and experience almost no additional acceleration during their flights (Varsani et al., 2017). We have indeed confirmed that these electrons are originally accelerated near the EDR and experience no additional significant acceleration and drifting during their propagation to the probe (not shown). This is a typical feature of the first contact of reconnection signatures at the reconnection boundary at a location sufficiently far away from the X-line as very recently observed by MMS at the near-Earth PSBL (Varsani et al., 2017). The P4 probe observes similar signatures $\Delta t = 2\Omega_i^{-1}$ later than P3 (see the time difference between two vertical lines in Figures 3g–3l). Substituting this Δt, the separation Δz, and the observed convection velocity (cyan lines in Figure 3l) into equation (3), E_r is estimated as shown in blue marks in Figure 2e, which is also reasonably consistent with the measured rate at the X-line. Similar to the red marks for the P1-P2 pair, the times of the two marks correspond to the times of the two vertical lines shown in Figures 3g–3l. The filled circle is the estimated E_r for the values observed at P3, while the open circle is for P4, and the difference of the two circles corresponds to the error of the estimation.

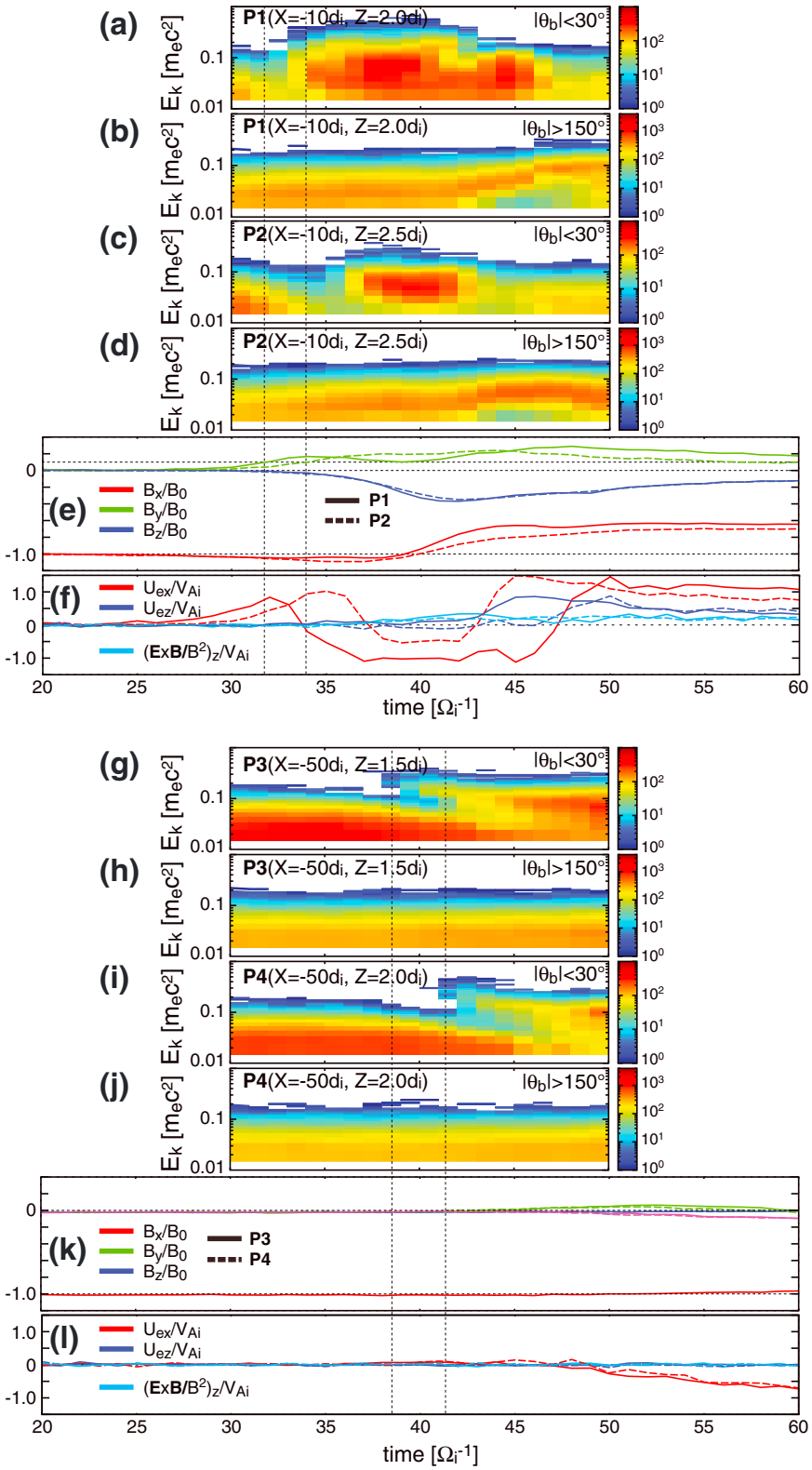

Figure 3. (a–f) Virtual observations for the probes P1 and P2 marked in Figures 2b–2d of (a–d) energy spectrograms for parallel (pitch angle $|\theta_b| < 30°$) and antiparallel ($|\theta_b| > 150°$) moving electrons, (e) three components of magnetic field **B**, and (f) *x* and *z* components of electron bulk velocity $\mathbf{U}_e$ and the *z* component of the convection velocity $\boldsymbol{V}_c = (\boldsymbol{E} \times \boldsymbol{B})/B^2$. (g–l) The same as Figures 3a–3f but for the probes P3 and P4.

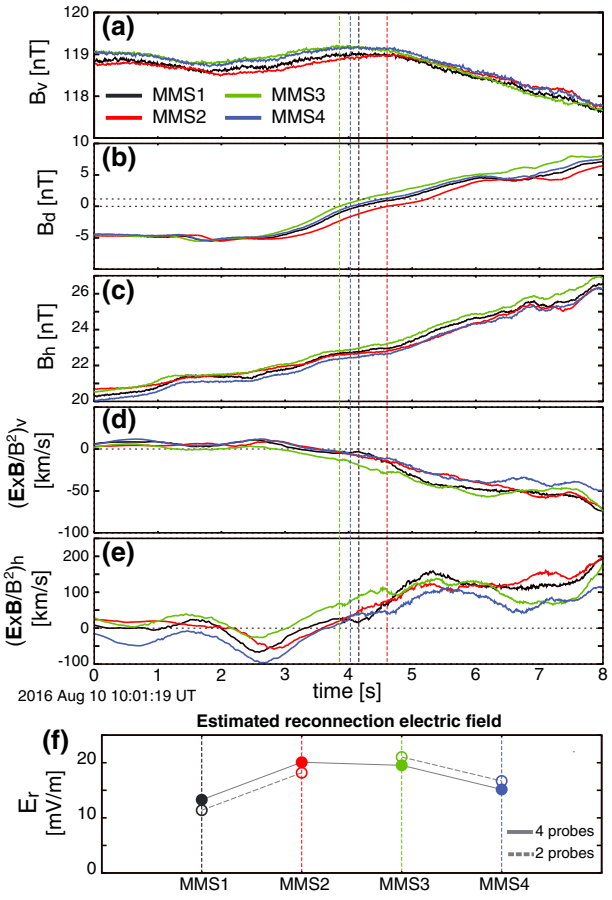

Figure 4. (a–e) MMS observations of the PSBL for 8 s from 10:01:19UT on 10 August 2016, which were first reported by Nakamura, Nagai, et al. (2017), Nakamura et al. (2018), of three components of magnetic field, and *v* and *h* components of the convection velocity $\boldsymbol{V}_c = (\boldsymbol{E} \times \boldsymbol{B})/B^2$ for all four spacecraft. Each vertical line in different color shows the timing of the $B_d = 0$ crossing for each spacecraft. The local VDH coordinate system is employed to better represent the reconnection (*VH*) plane (see Nakamura, Nagai, et al., 2017, for more details of the VDH coordinate descriptions). (f) Estimated reconnection electric fields from equation (3) using the timing velocities for all four spacecraft (solid) and two spacecraft pairs MMS1-2 and MMS3-4 (dashed).

4. Summary and Discussion

4.1. Summary

In this paper, we propose a technique to remotely estimate the reconnection electric field (or the unnormalized reconnection rate) from multipoint (more than two-point) in situ measurements at the reconnection separatrix boundary by calculating the difference between the timing velocity of the boundary and the convection velocity ($\mathbf{V}_{tim}$-$\mathbf{V}_c$) as described in section 2.1 and equation (3). We applied this technique to a 2-D fully kinetic simulation of antiparallel reconnection. The results showed that the reconnection electric field remotely estimated from virtual observations for both the Hall current encounter case (Figures 3a–3f) and the parallel electron beam encounter case (Figures 3g–3l) agree well with the rates directly measured at the X-line (Figure 2e for these two cases and Figure S2 for an additional Hall current encounter case). These results indicate that the remote sensing technique introduced in this paper would be applicable over the whole separatrix boundary filled with reconnection signatures. The extent of the applicable region increases with time when the fast parallel electron beam propagates outwardly from the vicinity of the X-line along the separatrix as shown in Figures 2b–2d.

4.2. Applications to MMS Observations

The remote sensing technique introduced in this paper requires (i) full magnetic and electric field data to obtain timing and convection velocities during an observation interval for the timing velocity and (ii) the condition that the field variations during the observation interval are negligible. The MMS spacecraft would be useful to satisfy these requirements with its burst mode high-resolution magnetic field (Russell et al., 2014) and electric field (Ergun et al., 2014; Lindqvist et al., 2014; Torbert et al., 2014) data and its small separation (10–100 km), which prevents large-scale field variations from being observed during the interval wherein the technique is applied. The high-resolution plasma particle data (Pollock et al., 2016) are also useful to identify the reconnection boundary.

As the first attempt to apply the technique to the MMS observations, this paper features an event on 10 August 2016, in which the MMS spacecraft crossed the near-Earth ($X_{gsm} \sim -7R_e$) magnetotail region in the southern hemisphere and observed multiple dipolarizations as first reported by Nakamura, Nagai, et al. (2017), Nakamura et al. (2018). In this event, the four spacecraft first crossed the southern PSBL from the steady pure lobe region into the energetic reconnection region at around 10:01–10:02UT. Figure 4 zooms this PSBL crossing interval for 8 s from 10:01:19UT. We here employ the VDH coordinates as also employed in Nakamura, Nagai, et al. (2017), Nakamura et al. (2018), in which *H* is the component along the geomagnetic dipolar axis and is positive northward, *D* is perpendicular to *H* and the radial direction and is positive eastward, and *V* closes the right-hand coordinate system and is positive radially outward direction. In this system, the VH plane corresponds to the reconnection plane (roughly corresponding to *x*-*z* plane in the simulation shown in section 3), while *D* corresponds to the out-of-plane direction (*y* in the simulation). Before $t \sim 2$ s in Figures 4a–4e, steady pure lobe signatures were observed, while after $t \sim 2$ s, sharp positive B_d enhancements, which are the same polarities as the Hall field, were observed for all spacecraft (Figure 4b). We use this B_d enhancement as a representative signature of the reconnection boundary as discussed in Nakamura et al. (2018).

Since the northernmost MMS3 was the first spacecraft which entered the B_d enhancement interval and the southernmost MMS2 was the last one (compare green and red lines in Figure 4b), the overall direction of the motion of the reconnection boundary was southward. The timing velocities computed from the times of the $B_d = 0$ crossings observed by the MMS1-2 and MMS3-4 pairs in the *VH* plane are ($V_{tim,V}$, $V_{tim,H}$)

= ($\Delta V/\Delta t$, $\Delta H/\Delta t$) = (+24.3, −71.9) km/s and (−28.1, −110.3) km/s, respectively, which is roughly consistent with the velocity ($V_{tim,V}$, $V_{tim,H}$) = (34.27, −86.87) km/s from the timing method based on the four spacecraft shown in Nakamura et al. (2018). It is notable here that the H (north-south) component of the convection velocities (Figure 4d) for all four spacecraft were positive ($V_{c,H} \sim 50$ km/s)—the opposite sense to the timing velocities whose absolute values were comparable to or larger than the convection velocities (i.e., $V_{tim,H} < -V_{c,H} \sim -50$ km/s). Thus, during this crossing event, the reconnection boundary shifted southward more than two times faster than the northward convection of field lines (i.e., $(V_{tim,H}\text{-}V_{c,H}) < -2V_{c,H} \sim -100$ km/s), which may indicate a significant reconnection electric field.

Figure 4f shows the reconnection electric field estimated by substituting the above timing velocities $\mathbf{V}_{tim}$ for MMS1-2 and MMS3-4 pairs (dashed) and four spacecraft (solid) and the observed convection velocities $\mathbf{V}_c$ into equation (3). We took $\mathbf{V}_c$ at each $B_d = 0$ crossing for each spacecraft, and the estimated rate for each $\mathbf{V}_c$ is displayed in Figure 4f. The variations of the rates for two and four spacecraft correspond to the error of the estimation as shown in section 3.2. These estimation errors (~30%) would be more significant than instrumental errors in field measurements. The results show that the estimated E_r of this event is 15 ± 5 mV/m. This value could be 5–10 times higher than the typical value for the magnetotail reconnection in a fast reconnection regime ($R \sim 0.1$) $E_r \sim RV_AB_0/c \sim 2$ mV/m, where we take $B_0 = 20$ nT and $V_A = 1{,}000$ km/s (i.e., $n \sim 0.2$/cc) as typical values. Although there may be a possibility that a higher normalized rate ($R \gg 0.1$) led to the above higher E_r, this higher E_r can also be caused by a higher upstream V_AB_0 even in the fast reconnection regime ($R \sim 0.1$). Such high upstream V_AB_0 conditions could be caused, for example, by the reconnection region being filled with lower density (≪0.2/cc) lobe plasmas and/or by the externally added magnetic flux in the magnetotail (e.g., Birn & Hesse, 2007) resulting from a global magnetospheric convection (e.g., Hsu & McPherron, 2003; Pritchett, 2005). MHD simulations in Birn and Hesse (2007) indeed demonstrated that as the external flux increases, the upstream V_AB_0 increases, and consequently, E_r increases with almost no change of the normalized rate. Considering the fact that the observation time shown in Figure 4 was in the middle of the expansion phase of a very strong substorm with ~1,000 nT of the AE (auroral electrojet) index (see Figure 2 in Nakamura, Nagai, et al., 2017), the high E_r estimated in this paper may lead to (or be led by) such an intense substorm. A future statistical approach would be important for better understanding of the relation between the local reconnection electric field and the amplitude of geomagnetic disturbances.

Acknowledgments
This work was supported by the Austrian Research Fund (FWF): I2016-N20. The simulation employed in this research used resources at the Space Research Institute of Austrian Academy of Sciences. The observational portion of this research uses data from the MMS spacecraft. The MMS data are publically available via NASA resources and the Science Data Center at CU/LASP (https://lasp.colorado.edu/mms/sdc/public/). We thank T. Nagai, M. Hesse, R. Denton, J. Birn, H. Hasegawa, and N. Bessho for their fruitful discussions.

References

Birn, J., Drake, J. F., Shay, M. A., Rogers, B. N., Denton, R. E., Hesse, M., et al. (2001). Geospace Environmental Modeling (GEM) magnetic reconnection challenge. *Journal of Geophysical Research*, *106*, 3715–3719. https://doi.org/10.1029/1999JA900449

Birn, J., & Hesse, M. (2007). Reconnection rates in driven magnetic reconnection. *Physics of Plasmas*, *14*(8), 082306. https://doi.org/10.1063/1.2752510

Birn, J., Liu, Y.-H., Daughton, W., Hesse, M., & Schindler, K. (2015). Reconnection and interchange instability in the near magnetotail. *Earth, Planets and Space*, *67*(1), 110. https://doi.org/10.1186/s40623-015-0282-3

Blanchard, G. T., Lyons, L. R., & de la Beaujardie're, O. (1997). Magnetotail reconnection rate during magnetospheric substorms. *Journal of Geophysical Research*, *102*, 24,303–24,312. https://doi.org/10.1029/97JA02163

Burch, J. L., Moore, T. E., Torbert, R. B., & Giles, B. L. (2016). Magnetospheric Multiscale overview and science objectives. *Space Science Reviews*, *199*(1-4), 5–21. https://doi.org/10.1007/s11214-015-0164-9

Burch, J. L., Torbert, R. B., Phan, T. D., Chen, L.-J., Moore, T. E., Ergun, R. E., et al. (2016). Electron-scale measurements of magnetic reconnection in space. *Science*, *352*, 1189. https://doi.org/10.1126/science.aaf2939

Cassak, P. A., Liu, Y.-H., & Shay, M. A. (2017). A review of the 0.1 reconnection rate problem. *Journal of Plasma Physics*, *83*(05), 5. https://doi.org/10.1017/S0022377817000666

Chen, L.-J., Hesse, M., Wang, S., Gershman, D., Ergun, R. E., Burch, J., et al. (2017). Electron diffusion region during magnetopause reconnection with an intermediate guide field: Magnetospheric multiscale observations. *Journal of Geophysical Research: Space Physics*, *122*, 5235–5246. https://doi.org/10.1002/2017JA024004

Daughton, W., Scudder, J., & Karimabadi, H. (2006). Fully kinetic simulations of undriven magnetic reconnection with open boundary conditions. *Physics of Plasmas*, *13*(7), 072101. https://doi.org/10.1063/1.2218817

de la Beaujardière, O., Lyons, L. R., & Friis-Christensen, E. (1991). Sondrestrom radar measurements of the reconnection electric field. *Journal of Geophysical Research*, *96*, 13,907–13,912. https://doi.org/10.1029/91JA01174

Ergun, R. E., Tucker, S., Westfall, J., Goodrich, K. A., Malaspina, D. M., Summers, D., et al. (2014). The axial double probe and fields signal processing for the MMS mission. *Space Science Reviews*, *199*(1-4), 167–188. https://doi.org/10.1007/s11214-014-0115-x

Freeman, M. P., Chisham, G., & Coleman, I. J. (2007). Remote sensing of reconnection. In J. Birn & E. Priest (Eds.), *Reconnection of Magnetic Fields* (Chap. 4.6, pp. 217–228). New York: Cambridge University Press.

Fuselier, S. A., Petrinec, S. M., & Trattner, K. J. (2010). Antiparallel magnetic reconnection rates at the Earth's magnetopause. *Journal of Geophysical Research*, *115*, A10207. https://doi.org/10.1029/2010JA015302

Genestreti, K. J., Varsani, A., Burch, J. L., Cassak, P. A., Torbert, R. B., Nakamura, R., et al. (2018). MMS observation of asymmetric reconnection supported by 3-D electron pressure divergence. *Journal of Geophysical Research: Space Physics*, *123*, 1806–1821. https://doi.org/10.1002/2017JA025019

Hesse, M., & Winske, D. (1998). Electron dissipation in collisionless magnetic reconnection. *Journal of Geophysical Research*, *103*, 26,479–26,486. https://doi.org/10.1029/98JA01570

Hoshino, M. (1987). The electrostatic effect for the collisionless tearing mode. *Journal of Geophysical Research*, *92*, 7368–7380. https://doi.org/10.1029/JA092iA07p07368

Hsu, T.-S., & McPherron, R. L. (2003). Occurrence frequencies of IMF triggered and nontriggered substorms. *Journal of Geophysical Research*, *108*(A7), 1307. https://doi.org/10.1029/2002JA009442

Hubert, B., Milan, S. E., Grocott, A., Blockx, C., Cowley, S. W. H., & Gérard, J.-C. (2006). Dayside and nightside reconnection rates inferred from IMAGE FUV and Super Dual Auroral Radar Network data. *Journal of Geophysical Research*, *111*, A03217. https://doi.org/10.1029/2005JA011140

Karimabadi, H., Daughton, W., & Scudder, J. (2007). Multi-scale structure of the electron diffusion region. *Geophysical Research Letters*, *34*, L13104. https://doi.org/10.1029/2007GL030306

Lindqvist, P.-A., Olsson, G., Torbert, R. B., King, B., Granoff, M., Rau, D., et al. (2014). The spin-plane double probe electric field instrument for MMS. *Space Science Reviews*, *199*(1-4), 137–165. https://doi.org/10.1007/s11214-014-0116-9

Liu, Y.-H., Daughton, W., Karimabadi, H., Li, H., & Gary, S. P. (2014). Do dispersive waves play a role in collisionless magnetic reconnection? *Physics of Plasmas*, *21*(2), 022113. https://doi.org/10.1063/1.4865579

Liu, Y.-H., Hesse, M., Guo, F., Daughton, W., Li, H., Cassak, P. A., & Shay, M. A. (2017). Why does steady-state magnetic reconnection have a maximum local rate of order 0.1? *Physical Review Letters*, *118*(8), 085101. https://doi.org/10.1103/PhysRevLett.118.085101

Nagai, T., Shinohara, I., Fujimoto, M., Machida, S., Nakamura, R., Saito, Y., & Mukai, T. (2003). Structure of the Hall current system in the vicinity of the magnetic reconnection site. *Journal of Geophysical Research*, *108*(A10), 1357. https://doi.org/10.1029/2003JA009900

Nakamura, R., Nagai, T., Birn, J., Sergeev, V. A., Le Contel, O., Varsani, A., et al. (2017). Near-Earth plasma sheet boundary dynamics during substorm dipolarization. *Earth, Planets and Space*, *69*(1), 129. https://doi.org/10.1186/s40623-017-0707-2

Nakamura, R., Varsani, A., Genestreti, K. J., Le Contel, O., Nakamura, T., Baumjohann, W., et al. (2018). Multi-scale currents observed by MMS in the flow braking region. *Journal of Geophysical Research: Space Physics*, *123*, 1260–1278. https://doi.org/10.1002/2017JA024686

Nakamura, T. K. M., Eriksson, S., Hasegawa, H., Zenitani, S., Li, W. Y., Genestreti, K. J., et al. (2017). Mass and energy transfer across the Earth's magnetopause caused by vortex-induced reconnection. *Journal of Geophysical Research: Space Physics*, *122*, 11,505–11,522. https://doi.org/10.1002/2017JA024346

Nakamura, T. K. M., Nakamura, R., & Hasegawa, H. (2016). Spatial dimensions of the electron diffusion region in anti-parallel magnetic reconnection. *Annales de Geophysique*, *34*(3), 357–367. https://doi.org/10.5194/angeo-34-357-2016

Parker, E. N. (1957). Sweet's mechanism for merging magnetic fields in conducting fluids. *Journal of Geophysical Research*, *62*, 509–520. https://doi.org/10.1029/JZ062i004p00509

Petschek, H. E. (1964). Magnetic field annihilation. In H. Petschek (Ed.), *Proceedings of AAS-NASA symposium on the physics of solar flares* (pp. 425). Washington, DC: NASA.

Phan, T.-D., Sonnerup, B. U. Ö., & Lin, R. P. (2001). Fluid and kinetics signatures of reconnection at the dawn tail magnetopause: Wind observations. *Journal of Geophysical Research*, *106*, 25,489–25,501. https://doi.org/10.1029/2001JA900054

Pollock, C. J., Moore, T., Jacques, A., Burch, J., Gliese, U., Saito, Y., et al. (2016). Fast plasma investigation for Magnetospheric Multiscale. *Space Science Reviews*, *199*(1-4), 331–406. https://doi.org/10.1007/s11214-016-0245-4

Pritchett, P. L. (2001). Geospace Environment Modeling (GEM) magnetic reconnection challenge: Simulations with a full particle electromagnetic code. *Journal of Geophysical Research*, *106*, 3783–3798. https://doi.org/10.1029/1999JA001006

Pritchett, P. L. (2005). Externally driven magnetic reconnection in the presence of a normal magnetic field. *Journal of Geophysical Research*, *110*, A05209. https://doi.org/10.1029/2004JA010948

Russell, C. T., Anderson, B. J., Baumjohann, W., Bromund, K. R., Dearborn, D., Fischer, D., et al. (2014). The Magnetospheric Multiscale magnetometers. *Space Science Reviews*, *199*(1-4), 189–256. https://doi.org/10.1007/s11214-014-0057-3

Shay, M. A., Drake, J. F., & Rogers, B. N. (2001). Alfvenic collisionless magnetic reconnection and Hall term. *Journal of Geophysical Research*, *106*, 3759–3772. https://doi.org/10.1029/1999JA001007

Shay, M. A., Drake, J. F., & Swisdak, M. (2007). Two-scale structure of the electron dissipation region during collisionless magnetic reconnection. *Physical Review Letters*, *99*(15), 155002. https://doi.org/10.1103/PhysRevLett.99.155002

Sweet, P. A. (1958). The neutral point theory of solar flares. In B. Lehnert (Ed.), *Electromagnetic Phenomena in Cosmical Physics* (Vol. 6, pp. 123, 123–134). New York: Cambridge University Press. https://doi.org/10.1017/S0074180900237704

Torbert, R. B., Russell, C. T., Magnes, W., Ergun, R. E., Lindqvist, P. A., LeContel, O., et al. (2014). The FIELDS instrument suite on MMS: Scientific objectives, measurements, and data products. *Space Science Reviews*, *199*(1-4), 105–135. https://doi.org/10.1007/s11214-014-0109-8

Vaivads, A., Khotyaintsev, Y., André, M., Retinò, A., Buchert, S., Rogers, B., et al. (2004). Structure of the magnetic reconnection diffusion region from four-spacecraft observations. *Physical Review Letters*, *93*(10). https://doi.org/10.1103/PhysRevLett.93.105001

Varsani, A., Nakamura, R., Sergeev, V. A., Baumjohann, W., Owen, C. J., Petrukovich, A. A., et al. (2017). Simultaneous remote observations of intense reconnection effects by DMSP and MMS spacecraft during a storm time substorm. *Journal of Geophysical Research: Space Physics*, *122*, 10,891–10,909. https://doi.org/10.1002/2017JA024547

Vasyliunas, V. M. (1975). Theoretical models of magnetic field line merging. *Reviews of Geophysics*, *13*, 303–336. https://doi.org/10.1029/RG013i001p00303

Vasyliunas, V. M. (1984). Steady state aspects of magnetic field line merging. In E. W. Hones, Jr. (Ed.), *Magnetic Reconnection in Space and Laboratory Plasmas*, *Geophysical Monograph Series* (Vol. 30, pp. 25–31). Washington, DC: American Geophysical Union. https://doi.org/10.1029/GM030p0025